Detection in coincidence of gravitational wave bursts with a network of interferometric detectors: Geometric acceptance and timing

Nicolas Arnaud, Matteo Barsuglia, Marie-Anne Bizouard, Philippe Canitrot, Fabien Cavalier, Michel Davier, Patrice Hello, and Thierry Pradier

Laboratoire de l'Accélérateur Linéaire, Boîte Postale 34, Bâtiment 200, Campus d'Orsay, 91898 Orsay Cedex, France

(Received 28 February 2001; revised manuscript received 2 October 2001; published 25 January 2002)

Detecting gravitational wave bursts (characterized by short durations and poorly modeled waveforms) requires coincidences between several interferometric detectors in order to reject nonstationary noise events. As the wave amplitude seen in a detector depends on its location with respect to the source direction and as the signal to noise ratio of these bursts is expected to be low, coincidences between antennas may not be very likely. This paper investigates this question from a statistical point of view by using a simple model of a network of detectors; it also estimates the timing precision of a detection in an interferometer, which is an important issue for the reconstruction of the source location based on time delays.

DOI: 10.1103/PhysRevD.65.042004 PACS number(s): 04.80.Nn, 07.05.Kf

I. INTRODUCTION

In the next few years, the first generation of long baseline interferometric detectors of gravitational waves (GW's) will be operational [1–4]. Among the most promising sources of GW's, the compact binary inspirals and the periodic sources have already been studied for a long time (see [5] or [6] for a review); more recently, some analysis methods have been developed to look for GW bursts of short duration and unknown waveform, which are the subject of this paper.

Type II supernovae ([7] and references therein) and the merging phase of binary compact star and/or black hole systems [8] are the most common burst sources foreseen but others such as, e.g., cosmic strings [9] could also be considered promising. The lack of knowledge of such GW signals prevents us from using the optimal (Wiener) filtering method and requires suboptimal (i.e., less efficient yet robust) filters; various techniques have already been studied by different groups. The ''excess power statistics'' [10] monitors the power of the detector output with time and is shown to be optimal when minimal hypotheses (signal duration and bandwidth are the only known quantities) are taken into account [11]. Time-frequency methods have also been presented: the authors in [12] use the Wigner-Wille distribution to transform a time series into two-dimensional maps in which ridges are looked for by using the Steger algorithm; a Student-like test on noise periodograms has been studied in order to detect nonstationary events [13]. More generally, we have developed a set of filters able to be used as on-line triggers [14–16], the most promising being the ''alternative linear fit filter'' (ALF) [16], which aims at detecting a nonzero slope in data windows.

As burst signals are poorly modeled, only an accurate knowledge of the detector behavior could allow us to properly separate a real GW from nonstationarities in a single antenna; therefore, one will be more confident about the reality of a candidate event in the case of a significant coincidence between several interferometers, or between an interferometer and other types of detector (neutrinos, γ-ray satellites, etc.). Many studies in the literature assume such multidetections as the starting point of the analysis and deal with the ''inverse problem,'' i.e., how to extract information—source location in the sky, GW waveforms, astrophysical parameters—from these triggered data [17–19,21]. In this article we will not address this question, which will be the main topic of forthcoming papers aiming at developing coincidence strategies for the detection of bursts with a network of both GW antennas and detectors sensitive to other radiation such as neutrinos.

Simulations of massive star collapses [22,23] give typical GW amplitudes too low to expect a likely detection of sources outside the Galaxy; more optimistic estimates have been computed recently for the merging phase of two neutron stars [24] or a neutron star and a black hole [25], whose coalescences could be detected to 10 MPc given the planned sensitivity of the first generation of detectors. In both cases, as the GW amplitude is just above the noise level, the signal to noise ratios (SNR's) are nevertheless expected to be low, all the more that the wave amplitude detected in a given antenna depends on its location and orientation with respect to the source [5]: when the source direction is not orthogonal to the detector plane, the response to the GW is not optimal and so the SNR is decreased.

Therefore the feasibility and efficiency of coincidences between interferometers currently under construction worldwide is an important question: are these coincidences likely or not? This problem has so far attracted little attention in the literature, whereas it should be the starting point of the study of coincidence strategies: a precise knowledge on how a network of detectors surveys the sky is essential in defining the best possible methods to analyze their data.

This paper addresses this topic from a statistical point of view by performing Monte Carlo simulations of the detection process in a network of antennas. After describing the model used in the computations, we briefly recall the structure of the beam pattern functions—describing the interaction between a GW and a detector—and extract from them some information on the accuracy with which a particular sky direction is surveyed by a given interferometer. We will use the celestial sphere coordinates, i.e., the right ascension α and the declination δ to label sources. Sky maps will be constructed to characterize the detection power of each antenna and any combination of them.

Next, we introduce a quantity independent of any detec-

TABLE I. Detector data; all angles given in degrees.

Detector	Latitude l	Longitude L	Arm separation χ	Azimuth γ
VIRGO	43.6	−10.5	90.0	206.5
LIGO Hanford	46.5	119.4	90.0	261.8
LIGO Livingston	30.6	90.8	90.0	333.0
GEO600	52.3	−9.8	94.3	158.8
TAMA300	35.7	−139.5	90.0	315.0
AIGO	−31.4	−115.7	90.0	To be defined

tor, $\rho_{\max}$, characterizing a GW strength; the simulation results—detection probabilities for different configurations in the network: single antenna, twofold coincidence, threefold coincidence—are then presented either as functions of $\rho_{\max}$ and (α, δ) on a sky map, or simply versus $\rho_{\max}$ after averaging over all the sky directions.

Finally, the timing accuracy is strongly connected to the detection problem: reconstructing the source location in the sky or performing coincidences with other types of detector (γ rays, neutrinos, etc.) requires a good knowledge of the GW event timing in the interferometer(s). Therefore, we also present some results about the timing precision one can expect for typical burst detection before concluding.

II. MODELING THE DETECTION PROCESS IN A NETWORK OF INTERFEROMETERS

In this section we present the different hypotheses used in the Monte Carlo simulations whose results are presented below: first about the network of detectors; then we give some assumptions about the GW burst and the calibration of its amplitude; finally, we detail the detection process itself.

A. The network

Each detector D_i is described by a set of four angles: its latitude l_i, its longitude L_i, the angle between the two arms χ_i, and an orientation angle γ_i defined as the angle between the local South direction and the bisecting line of the detector arms counted counterclockwise. The values of these angles can be found in Table I extracted from [26], apart from those for AIGO [27].

The interferometer noise components are assumed to be white (after whitening [28,29] and applying line removal [31] methods), Gaussian, broadband, additive, and uncorrelated; lacking realistic sensitivities validated by measurements—this information will appear when detector runs start—we also assume they all have the same noise standard deviation σ and sampling frequency f_0.

The exact value of σ is of no importance as all the discussion of the paper is focused on SNR comparison. For example, by assuming a sampling frequency $f_0 = 20$ kHz (as in the VIRGO experiment) and a uniform one-sided spectral density $S_h \approx 16 \times 10^{-46}$/Hz (equal to the minimum of the foreseen VIRGO power spectrum), one finds from $\sigma \approx \sqrt{S_h f_0/2}$ a rms noise value of $\sigma = 4 \times 10^{-21}$.

Another assumption to be discussed is the choice of a stationary noise. As shown by data taken by prototypes of interferometric detectors, several noise features are likely to be present on top of Gaussian noise: power lines, long term drifts, transients, and so on (see, e.g., [30]). They imply a modification of the noise statistics and therefore a change in the response of detection algorithms. The main consequence is an increase of the false alarm rate with respect to the more ideal simulations.

One way to solve this problem would be to increase the trigger levels but this is quite unsatisfactory as it would lower the detection sensitivity. The nonstationarities must therefore be studied and then removed by some suitable sets of ''on-line'' algorithms before the data filtering. Some of them already exist [13,31,32] and others will be developed when real data are available in parallel with a better understanding of the interferometers. For the sake of simplicity, we assume in this paper that such a treatment is performed before the data analysis and so we do not take into account any non-Gaussian contribution in the detector noise.

B. The gravitational wave burst and the source direction

As a generic GW burst signal, we use a one-parameter set of Gaussian bursts

$$G_\tau(t) = K \exp\left(-\frac{t^2}{2\tau^2} \right), \tag{2.1}$$

where the width τ is taken between 0.1 and 10 ms and K is a scaling factor. Therefore, the maximum SNR (corresponding to an optimal detector orientation with respect to the source direction[1] and by using Wiener filtering), referred to as $\rho_{\max}$ in the following, is given by [14]

$$\rho_{\max} = K \frac{\pi^{1/4} \sqrt{f_0 \tau}}{\sigma}. \tag{2.2}$$

By assuming a value for $\rho_{\max}$, it is straightforward to compute K from Eq. (2.2) and so to characterize the amplitude of the GW burst independently of any detector.

Of course the real waveforms are not expected to be purely Gaussian but will present one or several peaks carrying a large fraction of the total signal. This justifies the use of

[1]This choice corresponds to what Thorne calls ''optimum source direction and polarization'' ([5], p. 37]). $\rho_{\max}$ is computed from the Wiener filtering theory by using the formula $\rho_{\max}^2 = (f_0/\sigma^2) \int G_\tau(t)^2 dt$.

Gaussian pulses in the present generic study. More definite studies could be performed for GW sources with well-modeled waveforms.

In addition to the two coordinates α and δ previously introduced, a third variable is necessary to determine completely the GW: the polarization angle ψ, one of the Euler angles describing the wave coordinate system in the transverse traceless gauge with respect to the celestial frame. In the simulations, unless specified otherwise, the GW sources are assumed to be uniformly distributed over the sky ($\alpha \in [-\pi;\pi]$, $\sin\delta \in [-1;1]$, $\psi \in [-\pi;\pi]$).

Finally, one has to note that the arrival time of the GW in the detectors is *a priori* not synchronized with the sampling, which will cause some losses in SNR and in timing accuracy for very narrow bursts.

C. The detection procedure

The detection method used is Wiener filtering—correlation with the known signal itself—for the sake of simplicity: it is an approximation of no consequence as an earlier paper [14] showed that the one-dimensional parameter space $[\tau_{\min}=0.1\ \text{ms};\tau_{\max}=10\ \text{ms}]$ can be covered by a discrete lattice of Gaussian filters ensuring a detection with a mismatch SNR loss lower than 1%. The threshold value on the filter output is set to $\eta=4.89$ which corresponds to a false alarm rate of 10^{-6}, i.e., 72/h for the VIRGO value of the sampling frequency f_0. This rather high value of the threshold is a compromise between a good detector sensitivity and a reasonable number of false alarms. Moreover, as soon as interferometers work together in a network, their thresholds can be lowered even more as coincident false alarms are really unlikely. For instance, assuming the same false alarm rate in two detectors (72/h) and an—overestimated—coincidence time window of 100 ms, one expects only 3.5 compatible false alarms a day.

One claims a detection if the filter output overcomes the threshold at least once in the analysis window. Decreasing the false alarm rate (10^{-7},10^{-8}, etc.) will not dramatically increase the threshold, so the results presented in the following remain essentially the same.

III. AVERAGED BEAM PATTERN SKY MAP

A. Beam pattern functions

In the frame associated with the GW (the wave direction being z by convention), in the TT gauge, the spatial metric perturbation is given by

$$H(t)=\begin{pmatrix} h_+(t) & h_\times(t) & 0 \\ h_\times(t) & -h_+(t) & 0 \\ 0 & 0 & 0 \end{pmatrix} \tag{3.1}$$

with h_+ and $h_\times$ corresponding to the two independent wave polarizations. By assuming the detector size small compared to the reduced wavelength of the GW [5] and by following the treatment presented, e.g., in [18,26], it is straightforward to show that the response $h(t)$ of an interferometric detector to this wave is a linear combination of the two polarizations:

$$h(t)=F_+(t)h_+(t)+F_\times(t)h_\times(t). \tag{3.2}$$

The corresponding weighting factors are called beam pattern functions; they have values in the range $[-1;\ 1]$ depending on the longitude and the latitude of the detector location, as well as its orientation, the angle between the interferometer arms χ, the sky coordinates $(\alpha,\ \delta)$ of the source, and the wave polarization angle ψ. Still following the notation and analysis of [26], one can compute the general expression for the beam pattern functions:

$$\begin{pmatrix} F_+(t) \\ F_\times(t) \end{pmatrix} = \sin\chi \begin{pmatrix} \cos 2\psi & \sin 2\psi \\ -\sin 2\psi & \cos 2\psi \end{pmatrix} \begin{pmatrix} a(t) \\ b(t) \end{pmatrix}. \tag{3.3}$$

The factor $\sin\chi$ recalls that the best response is achieved for detectors with orthogonal arms [such as, for instance, VIRGO and the two Laser Interferometric Gravitational Wave Observatory (LIGO) interferometers]; the a and b factors depend neither on ψ nor on χ and so 2ψ appears like a rotation angle and $\sin\chi$ like a scale factor for the beam pattern functions.

Because of the earth proper rotational motion the sky is in apparent motion with a period equal to a mean sidereal day. Therefore, the beam pattern functions associated with a source location $(\alpha,\ \delta)$ depend also on the UT t; let us introduce the local sidereal time $T(t)$ for a detector of longitude L:

$$T(t)=\kappa t+\Gamma_{\text{Greenwich}}(0)-L \tag{3.4}$$

with $\kappa \approx 1.0027379\times 15°/\text{h}$. $T_{\text{Greenwich}}(0)$ is the Greenwich sidereal time at 0 h UT and the minus sign before L comes from the fact that longitudes are counted positive westward. Then one can define the local hour angle of the source:

$$\mathfrak{h}(t)=T(t)-\alpha=\kappa t-(\alpha+L)+T_{\text{Greenwich}}(0). \tag{3.5}$$

Extensive calculations yield the complete expressions for a and b (depending on $\alpha,\ \delta,\ l,\ L,\ \gamma$, and t); we recall them for the sake of completeness even though they are completely equivalent to those presented in Sec. 2.1 of [26] (see also the references therein):

$$\begin{aligned} a(t)=&-\tfrac{1}{16}\sin 2\gamma(3-\cos 2l)(3-\cos 2\delta)\cos 2\mathfrak{h}(t) \\ &-\tfrac{1}{4}\cos 2\gamma \sin l(3-\cos 2\delta)\sin 2\mathfrak{h}(t) \\ &-\tfrac{1}{4}\sin 2\gamma \sin 2l \sin 2\delta \cos\mathfrak{h}(t) \\ &-\tfrac{1}{2}\cos 2\gamma \cos l \sin\mathfrak{h}(t)-\tfrac{3}{4}\cos 2\gamma \cos^2 l \cos^2\delta, \end{aligned} \tag{3.6}$$

$$\begin{aligned} b(t)=&-\cos 2\gamma \sin l \sin\delta \cos 2\mathfrak{h}(t)+\tfrac{1}{4}\sin 2\gamma \\ &\times(3-\cos 2l)\sin\delta \sin 2\mathfrak{h}(t) \\ &-\cos 2\gamma \cos l \cos\delta \cos\mathfrak{h}(t) \\ &+\tfrac{1}{2}\sin 2\gamma \sin 2l \cos\delta \sin\mathfrak{h}(t). \end{aligned} \tag{3.7}$$

B. Detector sky maps

The main interest in studying beam pattern functions is to characterize the sensitivity of an interferometric detector for different directions in the sky, independently of its noise

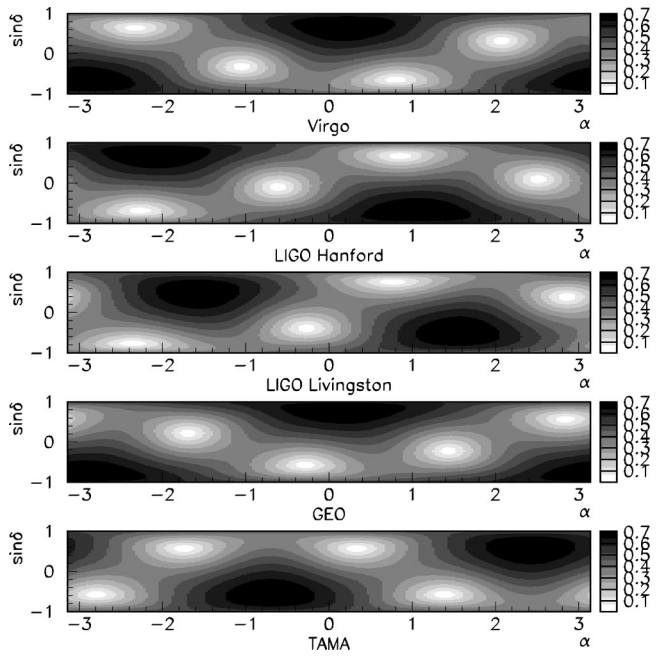

FIG. 1. Comparison of the beam pattern maps averaged over the polarization ψ for the six detectors of the network: VIRGO, LIGO Hanford and Livingston, GEO600, TAMA300, and AIGO. The AIGO orientation $\gamma_{\mathrm{AIGO}}=0°$, not currently specified, has been roughly optimized by Monte Carlo simulations.

curve. This can be done by performing a quadratic average of the beam pattern amplitude over the unknown polarization angle ψ. It leads to a ψ-independent quantity[2] $\overline{F}(t)$ given by

$$\overline{F}(t)=\frac{\sin\chi}{\sqrt{2}}\sqrt{a^2(t)+b^2(t)}\in\left[0;\frac{1}{\sqrt{2}}\right]. \tag{3.8}$$

We choose to present the variations of $\overline{F}$ in a two-dimensional contour plot figure—the ''sky map''—where any direction is located by a couple $(\alpha,\sin\delta)\in[-\pi;\pi]\times[-1;1]$. For a given detector, $\overline{F}$ depends not only on α and δ but also on the time t. For the sake of simplicity, each sky map shown below in the paper is determined at the time $t=t_0$ defined by $\kappa t_0+T_{\mathrm{Greenwich}}(0)=0[2\pi]$; to have results at another time t one can simply imagine the map on a cylinder whose axis is along the sin δ direction and rotate it by $\delta\mathfrak{H}(t)=\mathfrak{H}(t)-\mathfrak{H}(t_0)$.

Figure 1 compares the sky maps of the ψ-averaged beam pattern function $\overline{F}$ for the six interferometers currently in development or planned in the world: VIRGO, the two LIGO antennas, GEO600, TAMA300, and AIGO. In each case, the $\overline{F}$ averaged value over the whole sky is 0.42 and the rms is 0.16; each map presents two maxima corresponding to directions that are orthogonal to the detector plane and four minima (direction of the bisector of the two arms and its three images by rotations of angles $\pi/2$, π, and $3\pi/2$ in the detector plane) included in a large ''valley'' where $\overline{F}$ remains quite small.

To simplify the analysis presented in this paper we now consider only three of these antennas as this is the minimum number required in order to be able to reconstruct the source direction in the sky in case of a full coincidence. We keep the two LIGO interferometers as they have been planned to work coherently by construction and as they have the same design sensitivities; VIRGO and GEO600 have almost identical $\overline{F}$ sky maps (at least for the areas where the averaged beam pattern function is maximal) and so keeping one of the two (retaining VIRGO which is expected to have a sensitivity similar to LIGO) is enough to compute the main properties of an American-European network. Finally, even though the TAMA300 sky map is different from the other ones, its expected sensitivity is too small—with respect to the other antennas previously mentioned—to help the network detection. So, in the following and in Sec. IV, the network chosen is made of three detectors: VIRGO (V) and the two LIGO interferometers in Hanford (H) and Livingston (L); the selected antennas are those expected to achieve the best broadband sensitivities. Nevertheless, the results presented in this paper can be easily extended to accommodate additional interferometers into the network as shown in Sec. V.

The regions of maximum $\overline{F}$ are rather close for the two LIGO interferometers but quite different from those of VIRGO. Therefore one can expect on one hand a good complementarity between the three interferometers for a single detection—a clear advantage to maximize sky coverage. On the other hand, the ability to perform coincidences among the three detectors is expected to be significantly reduced—at least for small SNR values.

C. Daily averaging

As mentioned before, the two-dimensional maps previously defined are also functions of time. Therefore, another way to present the information they contain is to average $\overline{F}$ over one sidereal day (and so over α) and keep only the dependence in the declination variable sin δ:

$$(\overline{F})^{\mathrm{averaged}}(\sin\delta)=\frac{1}{2\pi}\int_{-\pi}^{\pi}d\alpha\,\overline{F}(\alpha,\sin\delta). \tag{3.9}$$

Figure 2 presents the graphs of $(\overline{F})^{\mathrm{averaged}}$ for the three detectors VIRGO, LIGO Hanford, and LIGO Livingston. Note that the vertical axis scale is zero suppressed to enhance the variations which are in fact small ($\lesssim$30%) around the mean value of 0.42. Due to the successive averages, these plots mainly depend on the detector's latitude, which explains why the VIRGO and LIGO Hanford curves are quite similar. To make this figure more concrete, vertical lines are given corresponding to the locations of some centers of galaxies where GW sources are expected to be found: the Galaxy, the Magellanic clouds, M31 Andromeda, and M87 in the

[2]Because of this procedure it is no longer possible to separate ''+'' and ''×'' polarizations and thus the averaged values are equal for the two beam pattern functions. This definition of $\overline{F}$ may seem to be somewhat arbitrary but it is well correlated with the detection probability as shown by results given later in the paper.

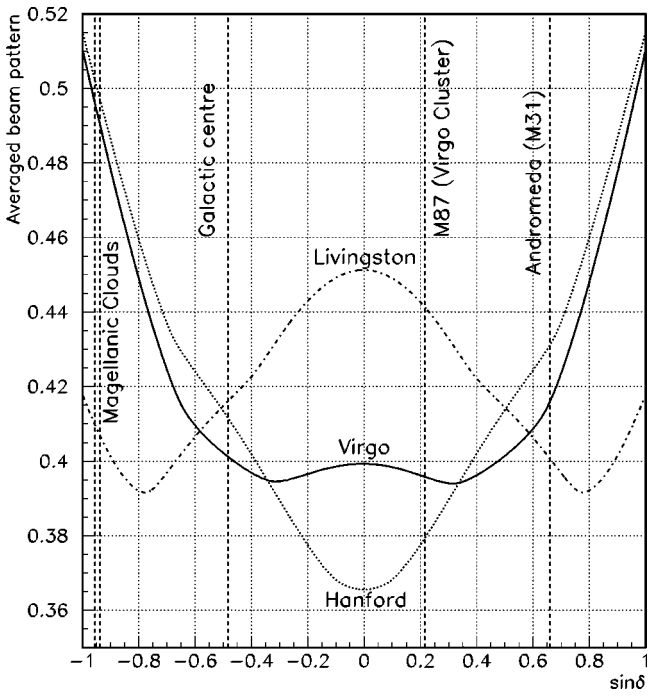

FIG. 2. Daily averaged $\overline{F}$ for the three detectors VIRGO and the two LIGO interferometers; the vertical dashed lines correspond to the location of some galaxy centers: the Galaxy, Magellanic clouds, Andromeda M31, and M87, one of the biggest components of the Virgo cluster.

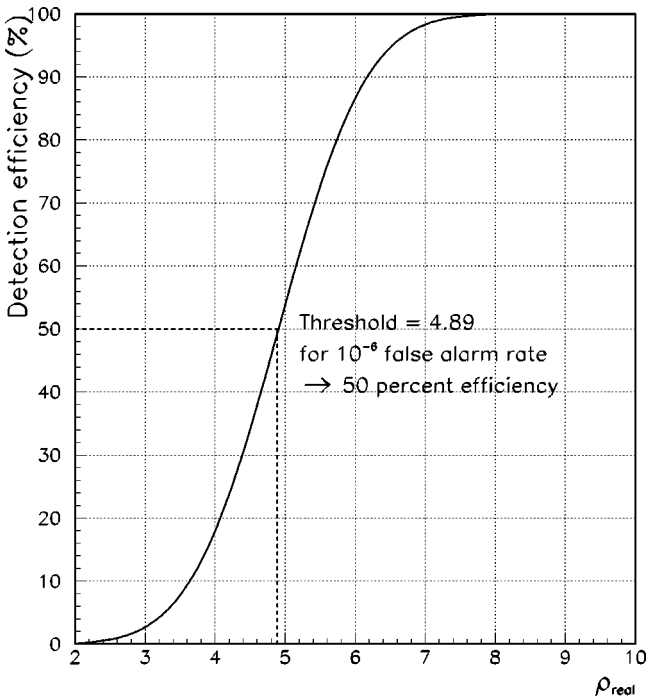

FIG. 3. Detection efficiency versus ρ_{real} for a false alarm rate of 10^{-6}.

Virgo cluster. For the galactic center and M31, the three detectors are roughly identical whereas Livingston is better for M87 and VIRGO/Hanford for the Magellanic clouds.

IV. DETECTOR CONFIGURATIONS

The detection process (whether exceeding a threshold or not) is not linear; therefore, it can only be studied by using Monte Carlo simulations. So, in the following, no *a priori* average on ψ is performed; we assume uniform distributions of sources in the sky which correspond to the ranges of variables quoted in Sec. II B. The results are twofold: detection efficiencies versus ρ_{max} averaged over α, sin δ, and ψ; detection sky maps, i.e., detection probability versus (α, sin δ) for a given ρ_{max}, averaged on ψ. Various configurations are studied, from a single interferometer to the search for full coincidences between VIRGO and the two LIGO antennas.

A. Single detector

1. The example of VIRGO

As shown in Sec. III A, the amplitude of the GW interacting with a detector has to be multiplied by the beam pattern function with respect to the ideal case (optimal incidence and polarization). Therefore the signal to noise ratio is lowered by the same factor: let us denote by ρ_{real} the product $F \times \rho_{\mathrm{max}}$, where F is the beam pattern function. Figure 3 presents the detection efficiency as a function of the real signal to noise ratio ρ_{real} for a linear filter with a 10^{-6} false alarm rate. This efficiency is simply given by $\frac{1}{2}\,\mathrm{erfc}[(\eta - \rho_{\mathrm{real}})/\sqrt{2}]$ where η is the corresponding threshold and erfc the complementary error function.

The 50% efficiency is reached for ρ_{real}=threshold$\approx$5 and the detection is almost always successful for real SNR's higher than 7 (efficiency higher than 98%). Note that this curve obviously does not depend on the beam pattern.

Adding the effect of the nonoptimal detector response gives graphs such as those shown in Fig. 4. For two values of ρ_{max}—10 and 20—and a Gaussian width of τ=1 ms, one sees the following; continuous line—the distribution of ρ_{real} for ρ_{max} constant; this curve shape is due only to the beam pattern; and dashed line—the fraction of events really detected, computed by including the detector efficiency from Fig. 3. From 0 to $\rho_{\mathrm{max}}/2$ the distribution of ρ_{real} is flat; for higher values, it decreases monotonically up to the maximal signal to noise ratio. Adding the noisy detection process considerably lowers the number of events detected at small real SNR but keeps almost all those with $\rho_{\mathrm{real}} \geqslant 7$. By comparing the number of detected events with the total number of events generated by the Monte Carlo simulation, one can compute the detection efficiencies: 32% for ρ_{max}=10, 66% for ρ_{max}=20.

Simulating the real detection process, one obtains Fig. 5, which shows the detection probability versus ρ_{max} for different values of τ. As expected, this probability depends only on the signal to noise ratio, which is the relevant variable in signal analysis. Due to the beam pattern functions, the detection efficiency remains low even for large optimal signal to noise ratios: with ρ_{max}=10 the detection efficiency is only about 30%; it reaches 50% for ρ_{max}=14, and 90% for—unlikely—high values.

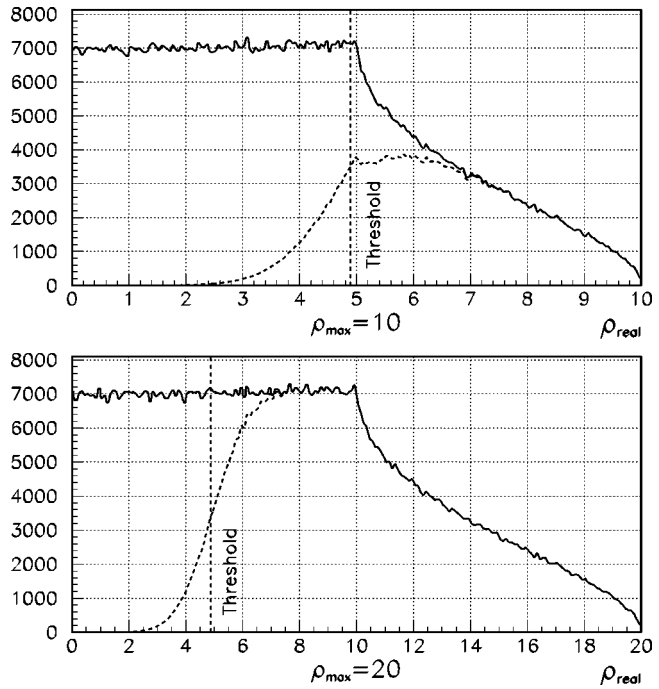

FIG. 4. Distribution of the real SNR of the GW burst assuming $\rho_{\max}=10$ or 20 and $\tau=1$ ms. The continuous line shows the SNR distribution due only to the beam pattern functions; the dashed line represents the final fraction of events detected by the filtering method computed by using the results shown in Fig. 3.

From these graphs one can conclude that including beam pattern functions in data analysis has major consequences on detection efficiency by greatly reducing the detection probability even for high $\rho_{\max}$.

The previous results deal with averaged efficiencies around the whole sky; of course, the detection probability depends on the relative position of the source with respect to the interferometer. Figure 6 presents the detection efficiencies versus (α, sin δ) for three values of $\rho_{\max}$. Note that these three maps are highly correlated with the upper graph of Fig. 1: $\overline{F}$ is thus a good—and easily computable—estimator of the detection probability in a given sky direction, especially in the low SNR region where the first detected events are likely to be located.

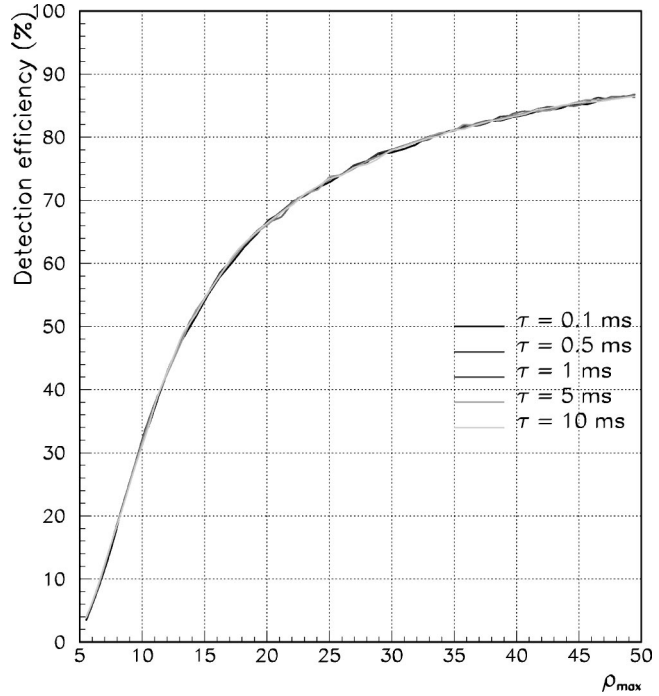

FIG. 5. VIRGO detection efficiency (in %) for different values of the width τ of the Gaussian signal as a function of $\rho_{\max}$.

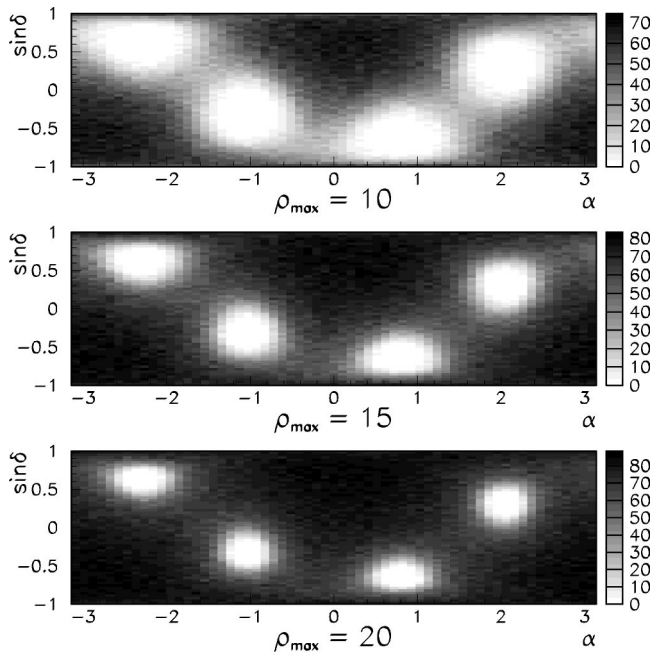

FIG. 6. Comparison of detection efficiency sky maps for three values of $\rho_{\max}$: 10, 15, and 20. The polarization angle ψ is randomly generated ensuring more realistic probabilities. Note the differences in the black/white code on the various graphs.

In the first case ($\rho_{\max}=10$), detections are possible for incoming wave directions almost orthogonal to the detector plane, considerably reducing the detection rate: a large fraction of the sky remains invisible. For $\rho_{\max}=15$ and 20, the detection probability is more uniform over the sky; the four minima are still there but they now cover narrower regions whose areas decrease as $\rho_{\max}$ increases. In the last case, there are simply blind islands among regions where the detection efficiency is larger than 60%.

Converting the results of these maps into fractions of sky with given detection probability leads to Fig. 7. One can note that especially at large $\rho_{\max}$ the fraction of sky covered decreases first slowly when the detection probability level increases and then more rapidly after some critical value. The reason for this evolution can be understood by looking at Fig. 6, considering the large part of the sky where the efficiency is large and almost constant. The detection probability is higher than 30% in 40% of the sky for $\rho_{\max}=10$; for $\rho_{\max}=15$ it is more than 50% in half of the sky; and it is almost 60% in 70% of the sky for $\rho_{\max}=20$. Therefore detections are likely for high maximal SNR $\rho_{\max}$ in any direction but even for $\rho_{\max}=20$ the efficiency never reaches 90%.

2. Daily averaged detection probability

This analysis can also be done for the two LIGO interferometers; as expected, averaging the detection probability

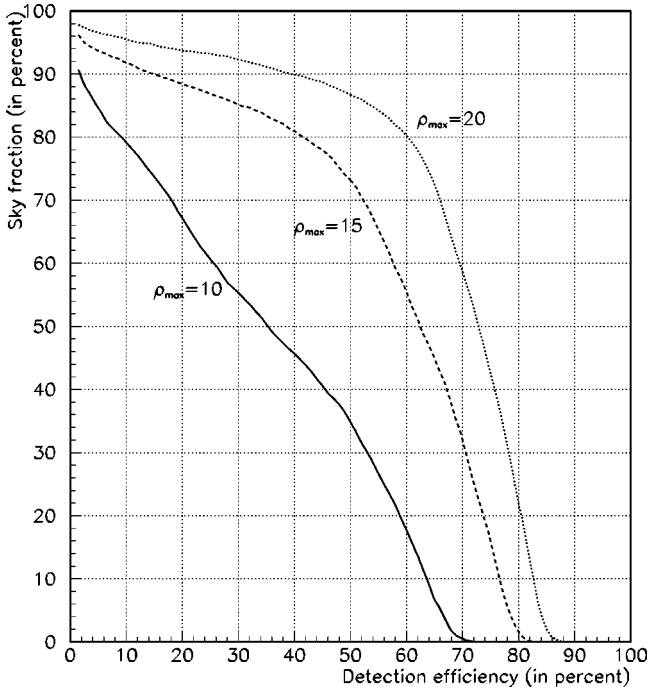

FIG. 7. Fraction of sky (in %) associated with a detection efficiency higher than a given value for $\rho_{\max}=10$, 15, and 20.

over the whole sky while taking $\rho_{\max}$ constant gives exactly the same results. To compare the three interferometers, we simply average on α over one day. Thus Fig. 8 shows the daily averaged detection efficiencies for each of the detectors and for three different values of the maximal signal to noise ratio, $\rho_{\max}=10$, 15, and 20. As in Fig. 2, the dashed vertical lines indicate some locations of galaxy centers. One can see

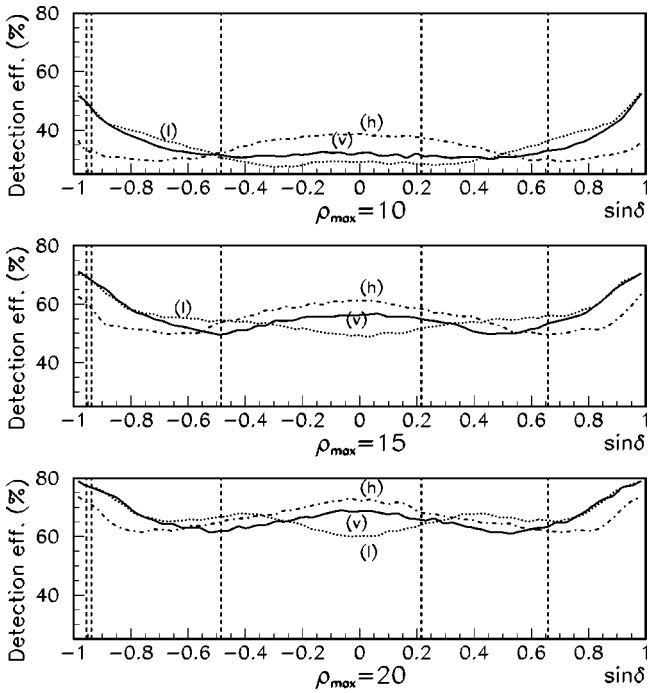

FIG. 8. Detection efficiency (in %) averaged over one day for the three detectors of the network and three values of $\rho_{\max}$: 10, 15, and 20.

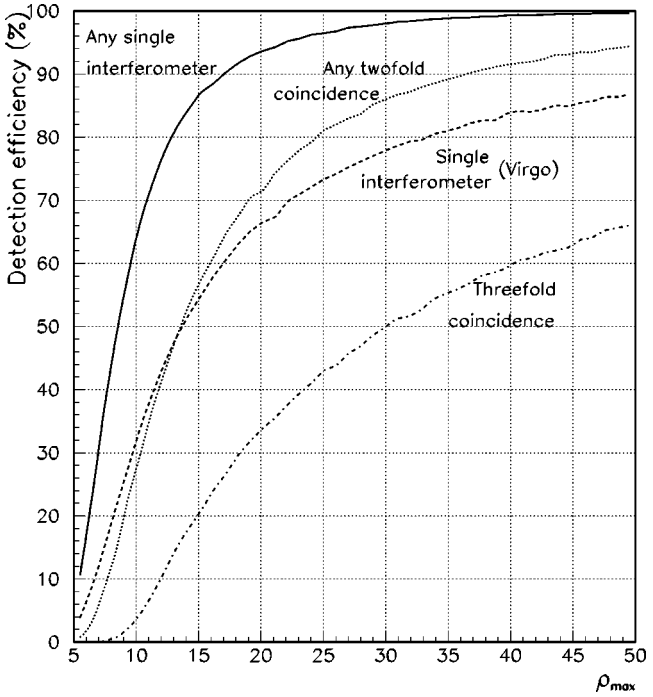

FIG. 9. Efficiency of detection (in %) for various network configurations of the VIRGO and the two LIGO interferometers. Continuous line, detection in at least one of the three interferometers; for comparison, dashed line recalls the detection efficiency in a single given interferometer. Dotted line, detection in at least two antennas; dot-dashed line, full coincidence in the three detectors.

that the detection probability is shifted to higher values for increasing $\rho_{\max}$; nevertheless, the curve shapes do not change too much and remain close to those shown in Fig. 2 for the averaged beam pattern functions: LIGO Livingston has the best results for small values of $|\sin\delta|$ whereas LIGO Hanford and VIRGO are more efficient for large $|\sin\delta|$. But there remain some differences between the two figures so that we should refine our previous statement: computing averaged beam pattern maps allows us to have an idea of the detection probability in different sky areas but it is necessary to perform Monte Carlo simulations including the detection process to compute the correct probabilities.

B. Detector complementarity

As we already checked that detection depends only on signal to noise ratio and not on the signal shape itself, we choose $\tau=1$ ms—a typical burst duration for the Gaussian waveform we use—in the following. In this section, we study the complementarity of the antennas, i.e., how their sky coverages complement each other, either for a single detection—the ''OR'' strategy—or for different types of coincidence—the ''AND'' strategies.

Figure 9 shows the detection probability versus $\rho_{\max}$ for different configurations of detectors in the network; the curve already presented in Fig. 5—single detector efficiency—is simply recalled for comparison. The continuous line shows the efficiency of detection in any single detector, i.e., the probability for a detection in at least one of the three interferometers. Network detection potential is clearly better than

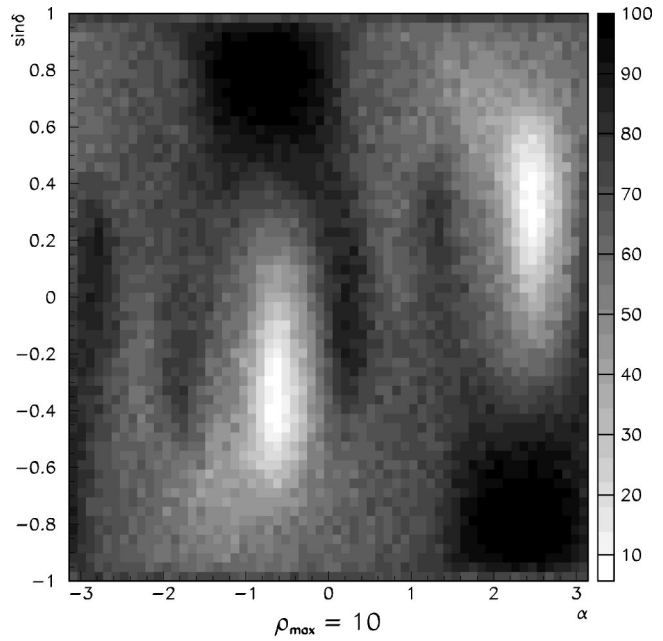

FIG. 10. Sky map of the detection efficiency in at least one of the three interferometers; ρ_{max} has been taken equal to 10.

for a single antenna and the smaller the ρ_{max} the higher the difference: more than twice more detections for $5 \leqslant \rho_{max} \leqslant 10$, more than 1.5 below $\rho_{max}=17$. The 50% efficiency is reached at $\rho_{max}=8$ and for $\rho_{max} \geqslant 15$ the probability is higher than 85% on average, corresponding to a likely detection in most parts of the sky.

On the same figure, one can also see the curve corresponding to a coincidence detection in at least two detectors among three ("OR" of twofold coincidences). For small values of ρ_{max}, the twofold coincidence probability remains lower than the detection efficiency in a single interferometer but above $\rho_{max}=13$—where the two compared probabilities are about equal to 50%—it becomes more likely to trigger in two detectors. Finally, the probability of full coincidence in the three interferometers of the network is considered. It is quite small for $\rho_{max} \leqslant 10$ and reaches useful levels only for very high maximal signal to noise ratios: the 50% efficiency is reached only for $\rho_{max}=30$.

To conclude this section, Fig. 10 presents the detection probability in at least one interferometer of the network ("OR" strategy) as a function of the source location in the sky. The maximal signal to noise ratio is set to 10 and so this graph can be compared with the top map of Fig. 6. The better efficiency achieved (about double, 67% on average instead of 34%) indeed corresponds to a more homogeneous detection probability over the sky.

In this section and the next more details are given on the coincidence probabilities as simultaneous detection in different interferometers will ensure much higher confidence levels for candidate events.

C. Twofold coincidences

Figure 11 shows the detection efficiencies for the three combinations of two detectors: VIRGO-Hanford, VIRGO-Livingston, and Hanford-Livingston. By construction, the association between the two LIGO antennas is always more efficient than between VIRGO and one of the LIGO interferometers. Nevertheless, the detection efficiency remains small: it is only 20% for the two LIGO antennas with $\rho_{max}=10$. One can therefore conclude that simultaneous detection in two given detectors is unlikely for weak GW signals and becomes likely ($\approx$40%) only for $\rho_{max} \geqslant 15$. The last graph of this figure presents the twofold coincidence detection probability in the network, when triggering occurs in at least two interferometers among the three. For the smallest values of ρ_{max} it corresponds to the two LIGO antennas case but then it increases more quickly: already at $\rho_{max}=10$ this probability is about 50% larger than for the two LIGO interferometers.

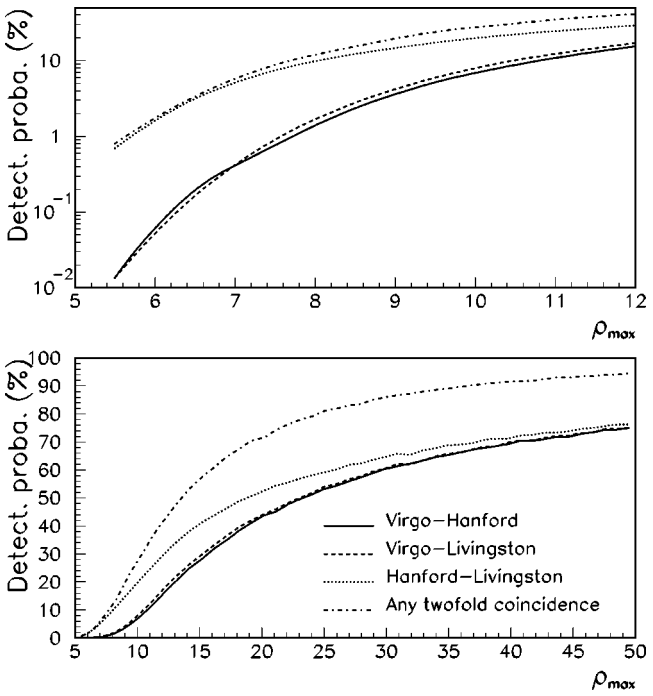

FIG. 11. Twofold coincidence detection probability. Bottom plot: full graph with $\rho_{max} \in [5;50]$. Top plot: Enlargement of area of small maximal signal to noise ratio values.

As the coincidence detection efficiency remains low for small values of ρ_{max} it is instructive to investigate how it is distributed over the sky. Figure 12 presents the detection efficiency of twofold coincidences versus $(\alpha, \sin\delta)$ for $\rho_{max}=10$—a likely value for the SNR of the first GW events detected. The three first maps are for the different twofold coincidences in the network while the fourth shows the detection probability in at least two detectors. One can see that, despite the differences in the black and white code of the graphs, the areas of high coincident detection probability are of small extent for the three configurations. In the last graph these regions are connected and the detection efficiency is higher, but nevertheless a major part of the sky remains invisible for the two-detector coincidences for low—but unfortunately realistic—ρ_{max} values.

D. Threefold coincidences

From the conclusions of the previous sections it is clear that a simultaneous detection in the three detectors is not

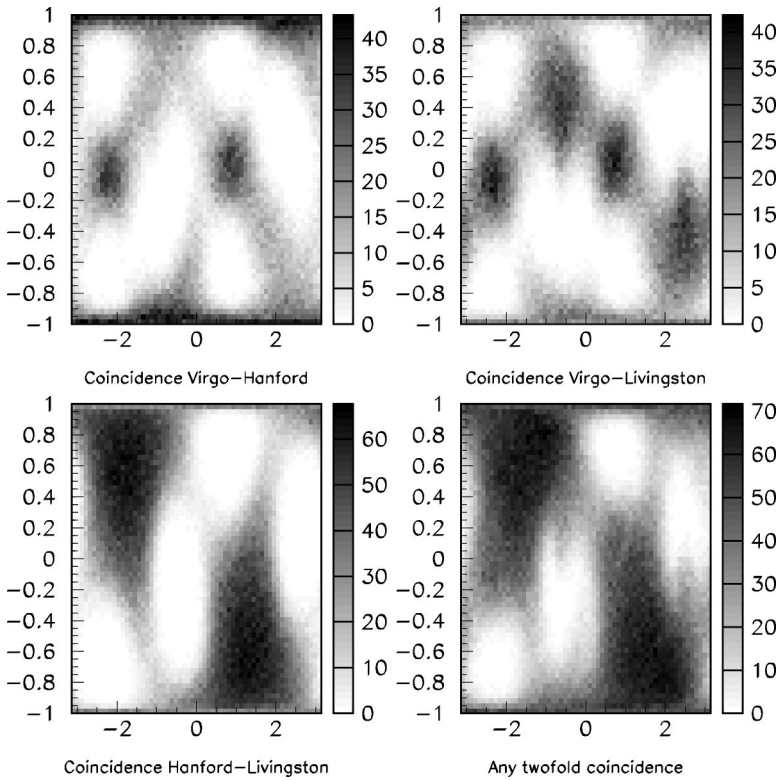

FIG. 12. Twofold detection efficiency sky maps computed with $\rho_{\max}=10$.

likely unless the optimal signal to noise ratio is large. Therefore it appears difficult to reconstruct GW astrophysical information from a source at the expected sensitivity level provided by the first generation of detectors.

Nevertheless, Fig. 13 shows the detection efficiency sky maps for values of the maximal signal to noise ratio of 10, 15, and 20, respectively. In the first case ($\rho_{\max}=10$), nonzero efficiency is concentrated in two small regions corresponding to the common visible areas of the LIGO-VIRGO combination, but even in these parts of the sky the detection efficiency is lower than 30%. In the two other cases, the distribution is more uniform with unfortunately some large areas that remain invisible—although they decrease as $\rho_{\max}$ increases.

V. TOWARD A MORE EXTENDED NETWORK OF INTERFEROMETERS

In this section we extend the previous study by including in the analysis other GW detectors located at the sites of GEO600, TAMA, and AIGO. For simplicity, we assume that they all have identical sensitivities. Such a situation may happen in some years when all these antennas are updated and/or replaced by second generation detectors. This hypothesis allows us to get a better understanding of the complementarity one can expect with the interferometers currently planned all around the world. The AIGO orientation has been chosen to maximize the six-interferometer network performance; Monte Carlo simulations showed that $\gamma_{\mathrm{AIGO}}\approx 0°$ is suitable.

Two aspects have been studied: (1) Which fraction of sources are detected by at least two (three, four) antennas among the six with respect to $\rho_{\max}$? (2) A comparison of the different networks corresponding to a given number of interferometers. The aim is to define some sets of detectors suitable for detection or for signal reconstruction (coincidences).

A. Full network performances

Figure 14 presents the detection performances of the extended network. The six curves show the probability of de-

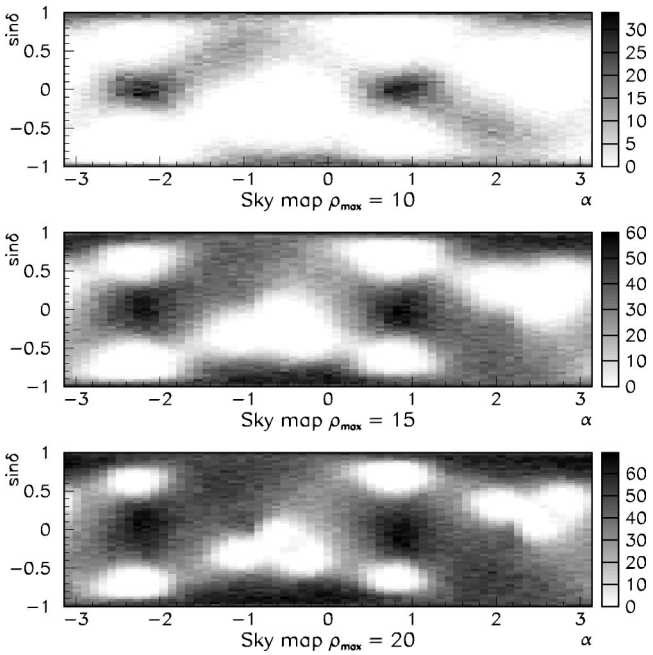

FIG. 13. Threefold coincidences: sky maps for three values of the optimal signal to noise ratio $\rho_{\max}=10$, 15, 20; note the differences in the black/white code of the various graphs.

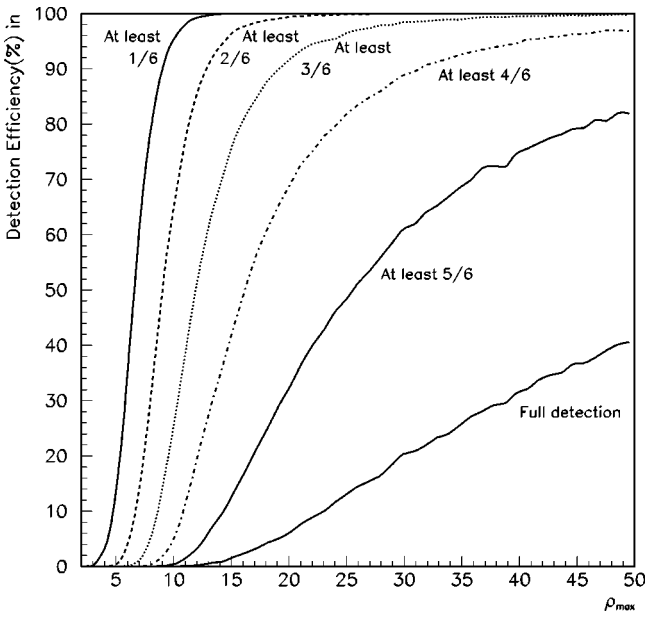

FIG. 14. Detection efficiency for the network of six interferometers.

tecting a signal in at least a given number of interferometers (from 1 to 6) versus the maximum SNR $\rho_{\max}$. As expected, the situation appears much more promising than with a smaller network.

First, for $\rho_{\max}=7$, the ''OR'' detection probability is already about 70% and becomes higher than 99% for $\rho_{\max}\geqslant 12$. For a single detector and for the Virgo-Hanford-Livingston network, the 70% efficiency is reached only at $\rho_{\max}$ values of 23 and 11, respectively; in those cases, a virtually certain detection occurs only for unlikely high values of the maximum SNR. The situation is also much better for coincidences as shown in Table II with two examples of coincidence aims. The first one, ''multiple detection,'' corresponds to a detection in at least two interferometers, which is the minimum necessary to claim a true astrophysical signal because of the detector noises. The second one is the possibility of extracting physical information from the coincidence—source location in the sky, GW polarizations—which implies that the SNR is higher than the threshold in at least three interferometers to allow some suitable triangulation. For these two possibilities, Table II gives the minimum values of $\rho_{\max}$ for which the detection efficiency exceeds some level.

For $\rho_{\max}\geqslant 16$,50% of the GW events are detected in four detectors or more, which allows a more precise analysis due to the redundancy of signals. Finally, detection in the complete network remains unlikely except for very large SNR values.

TABLE II. Minimal values of $\rho_{\max}$ needed to achieve a given level of detection efficiency for two coincidence scenarios.

Detection efficiency	50%	90%	95%
Multiple detection	9	13	15
Source location and GW polarization determination	12	20	23

TABLE III. Averaged detection probability versus the size of the network; $\rho_{\max}=5$.

Network size	1	2	3	4	5	6
Averaged detection efficiency (%)	3.8	7.5	11.2	14.7	18.2	21.3

B. Network comparison

Considering networks has interest only for coincidence detection. The differences between different sets of interferometers appear better with small values of $\rho_{\max}$: indeed, any detector is likely to trigger on a strong GW signal, not because it has a good location with respect to the source, but because of the signal strength itself. Therefore, this section deals only with small maximum SNR's, roughly $\rho_{\max}\leqslant 15$.

1. Two- and three-interferometer networks

As already mentioned, only two of the six interferometers—LIGO Hanford and LIGO Livingston—have been designed jointly. Therefore, it is not surprising that their association is by far the best of the two-detector networks: the twofold detection is more than twice bigger than the average value of the other networks for $\rho_{\max}=10$ and this difference remains around 30–40 % at $\rho_{\max}=15$. On the other hand, the network LIGO+LIGO has the worst results for a single detection: less than 50% of efficiency at $\rho_{\max}=10$ instead of about 60% for the other configurations. The close orientation of the two interferometers implies that they often both detect or *miss* a given source. Therefore, the two LIGO detectors are not sufficient by themselves for detection and the network must be extended.

The situation is similar for the three-interferometer networks. For instance, with $\rho_{\max}=10$, all the configurations with the two LIGO detectors miss more signals (32% on average instead of 22–26 % for the other networks) but have coincidences more often: about 30% of multidetections instead of 25%. These probabilities essentially do not depend on the choice of the third interferometer.

2. Larger interferometer network

For small values of $\rho_{\max}$—5 for instance—adding the interferometers in ''OR'' does not allow one to reach a much better sensitivity: the detector efficiency is only slightly better than 20% as the GW signal is too weak. Table III shows the detection probability averaged among all possible networks of a given size versus the number of detectors involved. Note that the results are roughly equal to the single detection probability times the number of interferometers: there are very few coincidence detections. On the other hand, for $\rho_{\max}\geqslant 10$, the situation is much more promising: with four interferometers, the detection efficiency is higher than 80% and reaches 90% for five detectors.

The particular connection between the two LIGO interferometers still appears even if it is reduced by the presence of other instruments in the network: when these two detectors are present, the no-detection probability is higher but coincidence detections are more likely. Apart from this particular

feature, the differences between networks are not very significant: configurations ''well distributed'' over the Earth (like, for instance, VIRGO/LIGO Livingston/TAMA/AIGO) have results very similar to networks chosen in a more ''random'' way. One can conclude that the number of interferometers used for a coincidence analysis is more important than their geographical locations for detection purpose. If the aim of the detection is to extract some physical information (GW timing, source location and nature, etc.), this conclusion is of course modified; it will be studied in a forthcoming article [36].

VI. TIMING RECONSTRUCTION

Determination of the absolute timing of a detected GW burst is an important question. First, coincidences in different antennas require time correlations between the respective detected signals. Secondly, the reconstruction of the source location is based only on arrival times detected in three detectors located in different places on Earth, and the better the precision, the smaller the angular error box in the sky. Thirdly, coincidences with other types of detector will also be based on time correlations. An application of the latter using neutrinos can be found in [33].

Let Δt be the time difference between the actual arrival time of the GW on the detector $t_{\rm real}$ and the reconstructed time $t_{\rm detect}$ corresponding to a detection with a given filter in the interferometer's output, when the SNR is maximal:

$$\Delta t = t_{\rm real} - t_{\rm detect}. \tag{6.1}$$

Generally speaking, there could be an offset between $t_{\rm real}$ and $t_{\rm detect}$ specific to the filter algorithm but here we assume it to be zero as would be obtained with matched filtering whose output peaks when the signal and the filter overlap.[3] Then the only significant parameter is the rms of the distribution $\Delta t^{\rm rms}$. *A priori* Δt can be split into two parts.

$\Delta t_{\rm sampling}$ due to the discrete data sampling of the experiments. For a signal of characteristic duration $\tau \gg 1/f_0$ it is completely negligible as it is well approximated by a uniform distribution in the range $[-1/2f_0; 1/2f_0]$ whose standard deviation is $1/\sqrt{12}f_0 \approx 1.4\times 10^{-2}$ ms, e.g., for VIRGO. But for signals of small duration it can become significant by randomly dropping high amplitude parts of the GW whose consequence would be to trigger off maximum (or to lose the event).

$\Delta t_{\rm noise}$ If the GW signal is embedded in detector noise, the precise location of the output highest value will depend on the actual noise time series; one expects this component to dominate for large τ. From dimensional analysis it is clear that Δt must be proportional to τ and so it is convenient to use the dimensionless quantity $\Delta t/\tau$.

[3]For the ALF filter—which is not designed for matched filtering and is not *a priori* well suited for precise timing—the time offset due to systematic and statistical errors is below 0.5 ms for typical supernovae waveforms [34].

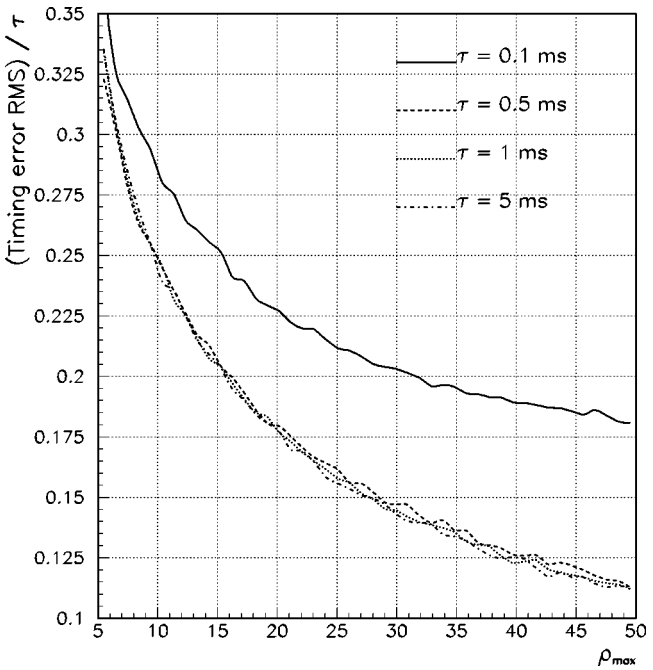

FIG. 15. Normalized timing error rms ($\Delta t^{\rm rms}/\tau$), τ being the Gaussian width, versus the maximal signal to noise ratio $\rho_{\rm max}$ and for five different values of τ between 0.1 and 10 ms.

Figure 15 shows the normalized rms $\Delta t^{\rm rms}/\tau$ as a function of $\rho_{\rm max}$ for different values of the Gaussian width τ. Apart from the case with $\tau = 0.1$ ms, which is sensitive to the finite sampling frequency as previously mentioned, all the other curves are identical.

From the data analysis point of view, it is mandatory to link the timing error with a measured quantity, the filter output ρ. The dependence of $\Delta t^{\rm rms}$ on this variable for τ values insensitive to the sampling rate can be represented by

$$\Delta t^{\rm rms} \approx \frac{1.45}{\rho}\left(\frac{\tau}{1\ {\rm ms}}\right). \tag{6.2}$$

The validity range of this equation is $\tau \gtrsim 0.2$ ms and the filter output $\rho \gtrsim 5-6$, as shown in Fig. 16 for a particular case, $\tau = 1$ ms and $\rho_{\rm max} = 20$: the fit curve and the real one are in good agreement from $\rho = 6$.

For $\tau = 1$ ms and a filter maximal output of about 10, one has $\Delta t^{\rm rms} \approx 0.1$ ms, which is well below a millisecond, the minimum level of precision suitable for coincidences with, for instance, neutrino detectors [35].

VII. CONCLUSIONS

This paper deals with the basic aspects of burst coincidence detection in a network of three gravitational wave antennas: VIRGO, LIGO Hanford, and LIGO Livingston. It does not focus on the signal parameter reconstruction—the inverse problem—but rather on studying the coincidence detection probability to see whether this kind of event is likely or not. In this respect, the results obtained are somewhat disappointing: the detection probability in a given interferometer is strongly reduced by the beam pattern

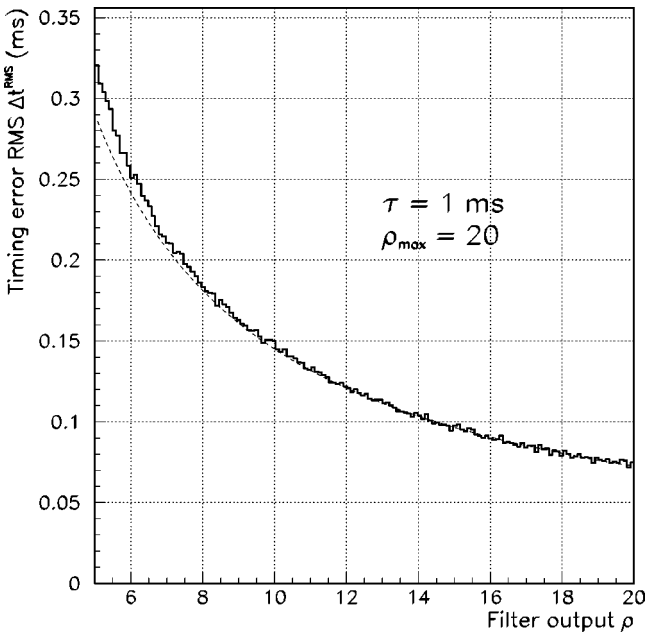

FIG. 16. Δt^{rms} versus ρ for $\tau=1$ ms and $\rho_{\max}=20$; the dashed line shows the fit value.

functions—on the average to only about 40%. We also show that there is a good complementarity between VIRGO and the two LIGO interferometers for detection (the ''OR'' strategy efficiency is higher than 50% for an optimal signal to noise ratio $\rho_{\max}\gtrsim 8$), but coincidences are very unlikely for weak signals.

Concerning twofold coincidences, the two-LIGO-antennas configuration has a much better detection efficiency compared to VIRGO with one of the LIGO interferometers (a factor of 2 larger for $\rho_{\max}=10$). Nevertheless, adding VIRGO and looking for any twofold coincidences allows the region of likely detection to be significally extended and the efficiency to be correspondingly increased: a 50% enhancement is obtained for $\rho_{\max}=10$, leading to a value averaged over the sky slightly higher than 30%. Finally, threefold coincidences between detectors are quite unlikely below the value $\rho_{\max}=30$ where 50% efficiency is reached.

As far as timing is concerned, the situation is quite satisfactory: Monte Carlo simulations show that the rms timing can remain below 1 ms even for low values of $\rho_{\max}$, which is an interesting point for coincidence with other kinds of detector. Even if the detection itself remains unlikely, the timing will be accurate enough if the GW is seen by the detectors.

The basic aspects covered in this paper about beam pattern functions and timing accuracy apply equally well to all transient sources whose characteristic times are much shorter than a day; in particular, this is the case for the coalescing binary signals that are expected to last from one second to a few minutes in the detector bandwidths. So coincidence analysis of binary inspirals will face the same detection efficiency problem as discussed for the bursts. Apart from this inescapable fact the situation of the data analysis is different here since the known binary signals can be searched for through matched filtering. This opens the possibility of ''coherent'' rather than ''coincidence'' analyses, as proposed in [19,20], which are shown [21] to give better results than a simple coincidence analysis; thus, this method may compensate for some of the geometric effects presented in this paper by using in an optimal way all the information available in the detectors. This improvement is made at the cost of a large increase in computing power since the source sky coordinates have to be included in the template definition. Therefore, despite the fact that it is suboptimal, coincidence analysis may be the only available tool in the first years of operation of the interferometers, even for binaries and especially for poorly modeled sources such as GW bursts.

One can *a priori* imagine two main strategies for their search.

(1) If the detector understanding is high enough to allow a proper elimination of nonstationary noise events, a burst detection is quite likely in at least one interferometer of the network since they cover the sky in a complementary way. Extending the number of sensitive antennas would further improve the detection efficiency. This situation is nevertheless not likely to arise in the first periods of data taking; it could even then be hopeless if the interferometer noise is not Gaussian. However, this strategy is well adapted to coincidences with non-GW detectors if they have a negligible false alarm rate [35].

(2) GW detection will in general require coincidences between interferometers. They may not be very frequent unless improvements are performed in the detector noise levels. Nevertheless, specific strategies must be devised in order to maximize sky coverage and detection efficiency [36].

The results presented in this article give an overview of the GW burst detectability in a network of antennas focusing only on the detection efficiency. To go beyond, it is necessary to take into account the corresponding false alarm rates and to compare all the available associations of detectors sensitive to GW's or other types of radiation such as neutrinos. Forthcoming papers will deal with these questions and also present new ideas about the ''inverse problem'' [35,36].

[1] A. Abramovici *et al.*, Science **256**, 325 (1992).
[2] B. Caron *et al.*, Nucl. Phys. B (Proc. Suppl.) **54B**, 167 (1997).
[3] K. Danzmann *et al.*, in *Gravitational Wave Experiments*, edited by E. Coccia, G. Pizzella, and F. Ronga (World Scientific, Singapore, 1995).
[4] K. Kuroda, in *Gravitational Waves: Sources and Detectors*, edited by I. Ciufolini and F. Fidecaro (World Scientific, Singapore, 1997).
[5] K. S. Thorne, in *300 Years of Gravitation*, edited by S. W. Hawking and W. Israel (Cambridge University Press, Cambridge, England, 1987).
[6] B. F. Schutz, in *The Detection of Gravitational Waves*, edited by D. G. Blair (Cambridge University Press, Cambridge, England, 1991).

[7] S. Bonazzola and J.-A. Marck, Annu. Rev. Nucl. Part. Sci. **45**, 655 (1994).
[8] K. Oohara and T. Nakamura, in *Relativistic Gravitation and Gravitational Waves*, edited by J.-A. Marck and J.-P. Lasota (Cambridge University Press, Cambridge, England, 1997).
[9] T. Damour and A. Vilenkin, Phys. Rev. Lett. **85**, 3761 (2000).
[10] E. E. Flanagan and S. A. Hughes, Phys. Rev. D **57**, 4535 (1998).
[11] W. G. Anderson *et al.*, Int. J. Mod. Phys. D **9**, 303 (2000).
[12] W. G. Anderson and R. Balasubramanian, Phys. Rev. D **60**, 102001 (1999).
[13] S. D. Mohanty, Phys. Rev. D **61**, 122002 (2000).
[14] N. Arnaud *et al.*, Phys. Rev. D **59**, 082002 (1999).
[15] N. Arnaud *et al.*, in ''Proceedings of the XXXIVth Rencontres de Moriond on Gravitational Waves and Experimental Gravity,'' Les Arcs, 1999, gr-qc/9903035.
[16] T. Pradier *et al.*, Phys. Rev. D **63**, 042002 (2001).
[17] Y. Gürsel and M. Tinto, Phys. Rev. D **40**, 3884 (1989).
[18] P. Jaranowski and A. Krolak, Phys. Rev. D **49**, 1723 (1994).
[19] S. Bose, A. Pai, and S. Dhurandhar, Int. J. Mod. Phys. D **9**, 325 (2000).
[20] A. Pai, S. Dhurandhar, and S. Bose, Phys. Rev. D **64**, 042004 (2001).
[21] L. S. Finn, Phys. Rev. D **63**, 102001 (2001).
[22] S. Bonazzola and J.-A. Marck, Astron. Astrophys. **267**, 623 (1993).
[23] T. Zwerger and E. Müller, Astron. Astrophys. **320**, 209 (1997).
[24] M. Ruffert and H.-Th. Janka, Astron. Astrophys. **338**, 535 (1998).
[25] H.-T. Janka, T. Eberl, M. Ruffert, and C. L. Fryer, Astrophys. J. Lett. **527**, L39 (1999).
[26] P. Jaranowski, A. Krolak, and B. F. Schutz, Phys. Rev. D **58**, 063001 (1998).
[27] D. Coward (private communication).
[28] M. Beccaria, E. Cuoco, and G. Curci, in *Proceedings of the Second Edoardo Amaldi Conference on Gravitational Waves*, Edoardo Amaldi Foundation Series Vol. IV, edited by E. Coccia, G. Pizzella, and G. Veneziano (World Scientific, Singapore 1998).
[29] E. Cuoco *et al.*, Class. Quantum Grav. **18**, 1727 (2001).
[30] B. Allen *et al.*, Phys. Rev. Lett. **83**, 1498 (1999).
[31] A. M. Sintes and B. F. Schutz, in *Gravitational Wave Detection II*, edited by Rie Sasaki (Universal Academy Press, Tokyo, in press).
[32] E. Chassante-Mottin and S. V. Dhurandhar, Phys. Rev. D **63**, 042004 (2001).
[33] N. Arnaud *et al.*, Phys. Rev. D **65**, 033010 (2002).
[34] T. Pradier, Ph.D. thesis, Orsay University, 2001. Available at the following URL: www.lal.in2p3.fr/presentation/bibliotheque/publications/Theses01.html
[35] N. Arnaud *et al.*, ''Detection in Coincidence of Gravitational Wave Bursts with a Network of Interferometric Detectors. II. Coincidences with Neutrino Detectors'' (in preparation).
[36] N. Arnaud *et al.*, ''Detection in Coincidence of Gravitational Wave Bursts with a Network of Interferometric Detectors. III. Strategies and Signal Reconstruction'' (in preparation).